FCH domain only-2 organizes clathrin-coated structures and interacts with Disabled-2 for low-density lipoprotein receptor endocytosis

Erin E. Mulkearns[a,b] and Jonathan A. Cooper[b]
[a]Molecular and Cellular Biology Program, University of Washington, Seattle, WA 98195; [b]Division of Basic Sciences, Fred Hutchinson Cancer Research Center, Seattle, WA 98109

ABSTRACT **Clathrin-mediated endocytosis regulates the internalization of many nutrient and signaling receptors. Clathrin and endocytic accessory proteins are recruited to receptors by specific adaptors. The adaptor Disabled-2 (Dab2) recruits its cargoes, including the low-density lipoprotein receptor (LDLR), and mediates endocytosis, even when the major adaptor protein AP2 is depleted. We hypothesized that the accessory proteins normally recruited by AP2 may be recruited by Dab2 if AP2 is absent. We identified one such accessory protein, the F-BAR protein FCH domain only-2 (FCHO2), as a major Dab2-interacting protein. The μ-homology domain (μHD) of FCHO2 binds directly to DPF sequences in Dab2 that also bind AP2. Disrupting the Dab2-FCHO2 interaction inhibited Dab2-mediated LDLR endocytosis in AP2-depleted cells. Depleting FCHO2 reduced the number but increased the size of clathrin structures on the adherent surface of HeLa cells and inhibited LDLR and transferrin receptor clustering. However, LDLR was internalized efficiently by FCHO2-deficient cells when additional time was provided for LDLR to enter the enlarged structures before budding, suggesting that later steps of endocytosis are normal under these conditions. These results indicate FCHO2 regulates the size of clathrin structures, and its interaction with Dab2 is needed for LDLR endocytosis under conditions of low AP2.**

Monitoring Editor
Robert G. Parton
University of Queensland

Received: Sep 26, 2011
Revised: Jan 23, 2012
Accepted: Feb 2, 2012

INTRODUCTION

Clathrin-mediated endocytosis (CME) is a major mechanism by which cells internalize nutrients, reorganize receptors, and regulate signaling (reviewed in Bonifacino and Traub, 2003; Conner and Schmid, 2003; Traub, 2003, 2009; McMahon and Boucrot, 2011). Receptors bind to endocytic adaptor proteins that also interact with clathrin and membrane phospholipids. These complexes then aggregate with clathrin into small patches of membrane. As the patches grow, accessory proteins responsible for membrane bending deform the lipid bilayer and the membrane begins to invaginate into a structure called a clathrin-coated pit (CCP). The CCP then grows and buds from the membrane, forming a sealed clathrin-coated vesicle (CCV), an event requiring the large GTPase dynamin and other accessory proteins. Coat and adaptor proteins are removed from the newly formed vesicle soon after internalization.

The adaptor protein AP2, historically considered a major "hub" for CCP assembly, binds to receptors containing dileucine or YxxΦ motifs, such as the transferrin receptor (TfnR; Bonifacino and Traub, 2003; Traub, 2003; Praefcke *et al.*, 2004). It also interacts with clathrin, the membrane phospholipid PtdIns(4,5)P_2, and many other accessory factors needed to form a functional CCP. Some of the accessory proteins known to interact with AP2 include the scaffolding proteins Eps15 and ITSN (Benmerah *et al.*, 1995; Hussain *et al.*, 1999), the membrane-bending BAR-domain protein amphiphysin (Wang *et al.*, 1995), dynamin (Wang *et al.*, 1995), and the

This article was published online ahead of print in MBoC in Press (http://www.molbiolcell.org/cgi/doi/10.1091/mbc.E11-09-0812) on February 9, 2012.
The authors declare no conflict of interests.

Address correspondence to: Jonathan A. Cooper (jcooper@fhcrc.org).

Abbreviations used: μHD, μ-homology domain; AP, adaptor protein; CCP, clathrin-coated pit; CCS, clathrin-coated structure; CCV, clathrin-coated vesicle; CHC, clathrin heavy chain; CLASP, clathrin-associated sorting protein; CME, clathrin-mediated endocytosis; Dab2, Disabled-2; DAPI, 4′,6-diamidino-2-phenylindole; DTT, dithiothreitol; FCHO2, FCH domain only-2; GFP, green fluorescent protein; GST, glutathione *S*-transferase; HBT, His-biotin tag; ITSN, intersectin; LCa-GFP, clathrin light chain-GFP; LC-MS/MS, liquid chromatography–tandem mass spectrometry; LDLR, low-density lipoprotein receptor; PTB, phosphotyrosine binding; PtdIns(4,5)P_2, phosphatidylinositol (4,5) bisphosphate; RT-PCR, reverse transcriptase PCR; shRNA, short hairpin RNA; siRNA, small interfering RNA; TfnR, transferrin receptor.

A

Protein Name	# of peptides
Dab2	203
HSPA1B	60
AP2B1*	57
FCHO2	46
AP2A1*	39
MyoVI*	34
ACOT9	28
CLTC*	27
AP2A2*	22
NUP155	22
SEC24B	20
PRDX1	18
AP2M1	18
MALT1	18
SF3B2	17
CCNT1	16
YLPM1	16
SEC23B	14
PYCR1	14
AURKA	13
C14orf166	13
SPSF6	13
HSPH1	12
TRIO	12
HNRNPL	12
AHCY	12
GRB2*	11
CPSF7	10
PS1TP5BP1	10

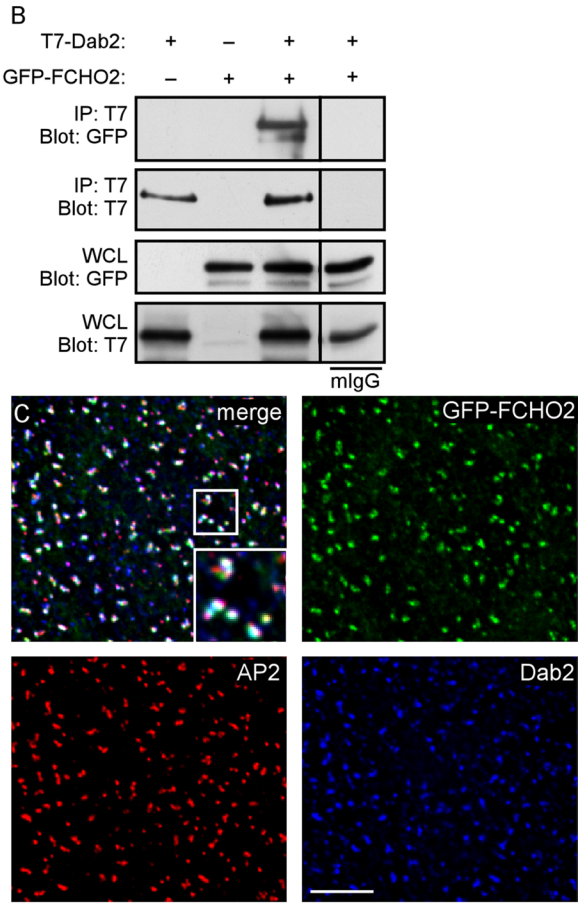

FIGURE 1: Dab2 interacts with FCHO2. (A) Proteins detected by MS from HBT-Dab2 purification. The total number of peptides is additive from two experiments. *, previously described interaction with Dab2. (B) Coimmunoprecipitation of GFP-FCHO2 with T7-Dab2 transiently expressed in HeLa cells. HeLa cells were lysed 48 h after transfection of GFP-FCHO2 and T7-Dab2 and subjected to immunoprecipitation with anti-T7. (C) HeLa cells transiently transfected with GFP-FCHO2 were fixed, permeabilized, and stained with antibodies to Dab2 and α-adaptin. White areas in the merge panel are places at which all three proteins colocalize. A 0.2-μm-thick section of the adherent surface of the cell is shown. Scale bar: 5 μm.

uncoating factor hsc70 (Praefcke *et al.*, 2004). In addition, AP2 binds to additional receptor-binding proteins, termed CLASPs, for clathrin-associated sorting proteins, to allow internalization of cargo with which AP2 cannot directly associate (Mishra *et al.*, 2005).

Disabled-2 (Dab2) is a CLASP that interacts with AP2 and recruits cargo to CCPs via its N-terminal phosphotyrosine-binding (PTB) domain (Morris and Cooper, 2001). Other members of the PTB-domain adaptor family include ARH and Numb. These adaptors bind FxNPxY motifs contained in receptors, such as the low-density lipoprotein receptor (LDLR; Morris and Cooper, 2001; He *et al.*, 2002; Mishra *et al.*, 2002b; Keyel *et al.*, 2006; Maurer and Cooper, 2006) and integrin β1 (Calderwood *et al.*, 2003; Nishimura and Kaibuchi, 2007; Teckchandani *et al.*, 2009). Dab2 can bind and assemble clathrin (Keyel *et al.*, 2006) and also associates with the motor protein myosin VI (Morris *et al.*, 2002) and the signaling adaptor Grb2 (Xu *et al.*, 1998).

LDLR internalization occurs through two partially redundant pathways utilizing either Dab2 or ARH. ARH requires AP2 to link to clathrin, but Dab2, at least under some conditions, can function in AP2-depleted cells (Motley *et al.*, 2003; Keyel *et al.*, 2006; Maurer and Cooper, 2006). It seems surprising that Dab2 can function in the absence of AP2, given the multitude of accessory proteins that are recruited by AP2 (Praefcke *et al.*, 2004; Schmid *et al.*, 2006). We reasoned that for Dab2 to function independently of AP2, Dab2 also might be able to recruit some of the same accessory proteins normally recruited by AP2.

In this paper, we report that Dab2 directly binds one such accessory protein, FCH domain only-2 (FCHO2). FCHO2 and its close relative FCHO1 contain F-BAR domains that bind to and tubulate membranes in vitro (Henne *et al.*, 2007; Reider *et al.*, 2009; Uezu *et al.*, 2011). The C-termini of FCHO proteins contain μ-homology domains (μHDs), which are similar to the AP2 μ2 subunit (Reider *et al.*, 2009). We detected FCHO2 in an unbiased screen for Dab2-binding partners and found that the Dab2-FCHO2 interaction site is needed for efficient endocytosis of LDLR when AP2-dependent endocytosis is inhibited. Depletion of FCHO2 inhibits endocytosis of the Dab2 cargo LDLR. FCHO2 depletion also inhibits assembly of CCPs and induces aggregates of CCP components that appear similar to clathrin plaques. Additional results suggest that FCHO2 is important for the early steps of endocytosis of Dab2-dependent and Dab2-independent cargoes.

RESULTS

Dab2 interacts with FCHO2

To identify Dab2-binding proteins, we used a mass spectrometry–based proteomics approach. The p96 form of mouse Dab2 was tagged with a His-biotin tag (HBT; Tagwerker *et al.*, 2006) and introduced into a line of HeLa cells in which Dab2 expression is stably inhibited with short hairpin RNA (shRNA; Teckchandani *et al.*, 2009). Cells infected with virus expressing only the HBT were used as a control. HBT and HBT-Dab2 protein were each sequentially purified over nickel and streptavidin beads and then subjected to SDS–PAGE. Proteins in sections of the gel were then analyzed by liquid chromatography–tandem mass spectrometry (LC-MS/MS). Twenty-nine proteins were detected in the Dab2 but not the HBT sample, in two separate experiments (Figure 1A). Strikingly, FCHO2 was the fourth most abundant protein detected. FCHO1 was not detected. We also found six proteins already known to interact with Dab2: four subunits of the AP2 complex (α1, α2, β1, and μ1; Morris and Cooper, 2001), myosin VI (Morris *et al.*, 2002), clathrin heavy chain (CHC; Mishra *et al.*, 2002a), and Grb2 (Xu *et al.*, 1998). Therefore the proteomics screen detected known and novel Dab2-binding proteins.

To confirm that Dab2 and FCHO2 interact in cells, we tested whether FCHO2 and Dab2 coimmunoprecipitated. FCHO2 and Dab2 were epitope-tagged with green fluorescent protein (GFP) and T7, respectively, and transiently expressed in HeLa cells. Cells were lysed and subjected to immunoprecipitation with antibody to T7. Immunoblotting revealed an ~130-kDa band that corresponded to the expected size for GFP-FCHO2 (Figure 1B). This confirms that FCHO2 and Dab2 interact in cells. Accordingly, immunofluorescence showed GFP-FCHO2 located in distinct cell surface puncta that colocalized with both Dab2 and AP2, indicating that FCHO2 localizes to clathrin-coated structures (CCSs) containing Dab2 and AP2 (Figure 1C). This localization pattern suggested that FCHO2 and its interaction with Dab2 were likely involved in some step of CME.

The Dab2 DPF motifs interact with the μHD of FCHO2

The N-terminus of Dab2 contains a PTB domain that interacts with PtdIns(4,5)P_2 and receptors containing the FxNPxY sequence (Morris and Cooper, 2001; Mishra *et al*., 2002a; Figure 2A). The central region of Dab2 is alternatively spliced; it is present in the p96 form but absent from a p67 splice form (Xu *et al*., 1995). This p96-specific central region contains two clathrin boxes (Mishra *et al*., 2002a), two NPF motifs that interact with EH domains (Di Fiore *et al*., 1997; Owen *et al*., 1999), and two DPF sequences that bind to AP2 (Morris and Cooper, 2001). The remainder of the protein, contained in both p67 and p96, includes another AP2-binding sequence, FLDLF (Brett *et al*., 2002; Mishra *et al*., 2002a), a site that binds myosin VI (Morris *et al*., 2002), three additional NPF motifs, and binding sites for SH3-domain proteins (Xu *et al*., 1995, 1998; Kowanetz *et al*., 2003; Zhou *et al*., 2003).

To map the region of Dab2 that binds FCHO2, we utilized wild-type p96, p67, and various p96 point and deletion mutants (Figure 2A). p96 and the NPF*, AP2*, DPF*, and FLDLF* mutants colocalized with AP2 in CCPs, whereas p67 and p96-ΔC were diffuse (Supplemental Figure S1; Morris and Cooper, 2001). T7-tagged Dab2 constructs were transfected into cells along with GFP-FCHO2 and were immunoprecipitated with anti-T7 antibody (Figure 2B). FCHO2 bound efficiently to p96 and to p96-ΔC, but not to p67, suggesting that FCHO2 binding requires the p96 central region but not the C-terminus. Mutating all five NPFs to NPV (NPF*) also did not affect binding. However, FCHO2 binding to Dab2 was disrupted by mutating the AP2-binding DPF sequences (Figure 2B, DPF*), but not by mutating the AP2-binding FLDLF sequence (Figure 2B, FLDLF*). Consistently, a compound mutant containing the DPF* and FLDLF* mutations also failed to bind FCHO2 (Figure 2B, AP2*). Previous studies suggested that the DPF and FLDLF sequences may be functionally redundant for binding AP2 (Morris and Cooper, 2001; Mishra *et al*., 2002a). Indeed, we found that p96 and the DPF* and FLDLF* mutants bound equally well to a glutathione *S*-transferase (GST)-tagged AP2 α-appendage ear domain in vitro (Figure 2C). These results suggest that the DPF motifs in Dab2 are required for binding to FCHO2, but not for binding AP2, provided that the FLDLF sequence is intact. Thus the DPF* mutant provides a tool for examining the importance of Dab2-FCHO2 interactions for endocytosis of Dab2-specific cargoes.

To determine which region of FCHO2 interacts with Dab2, deletion constructs of FCHO2 were created. GFP was fused to the N-terminus of the F-BAR domain (construct A), F-BAR and central region (construct B), central region alone (construct C), central and μHD (construct D), and μHD (construct E). Immunofluorescence showed that the μHD was necessary and sufficient for punctate localization and colocalization with AP2 in CCPs (Figure S2). The μHD was also necessary and sufficient for coimmunoprecipitation with T7-p96 (Figure 2D). While these experiments were under way, Dab2 was detected in a screen for FCHO2 μHD-binding proteins, confirming that Dab2 binds to the μHD (Henne *et al*., 2010). Together these data suggest that the μHD of FCHO2 is responsible for FCHO2 localization to CCPs and its interaction with the DPF motifs of Dab2.

To investigate whether the Dab2-FCHO2 interaction is direct, we produced T7-tagged FCHO2 μHD and the GST-tagged wild-type and AP2* central regions of Dab2 in bacteria and tested for binding in vitro. The FCHO2 μHD interacted with the central region of Dab2, and mutation of the AP2-binding sequences decreased binding (Figure 2E), indicating a direct interaction (Figure 2F).

FCHO2 and the other known μHD-containing proteins SGIPα, Syp1p, and FCHO1 also bind to the endocytic scaffolding and EH domain–containing protein Eps15 (Uezu *et al*., 2007, 2011; Reider *et al*., 2009; Henne *et al*., 2010). Because Dab2 is also able to interact with Eps15 and the additional EH-domain protein intersectin (ITSN; Teckchandani and Cooper, unpublished results), Dab2 could potentially also interact with FCHO2 indirectly, using Eps15 or ITSN as an intermediate. To determine whether this might be an alternative mechanism for Dab2-FCHO2 interaction, we repeated the Dab2-FCHO2 coimmunoprecipitation in cells that had been transfected with small interfering RNA (siRNA) to four endocytic EH-domain proteins: Eps15, Eps15R, ITSN1, and ITSN2. There was no change in the amount of FCHO2 that coimmunoprecipitated with Dab2 from cells depleted of EH-domain proteins (Figure S3). Eps15 and ITSN are therefore not required for the FCHO2-Dab2 interaction.

The Dab2-FCHO2 binding site is required for normal levels of LDLR endocytosis when AP2 is depleted

We made use of the DPF* Dab2 mutant to test whether the interaction of Dab2 with FCHO2 is required for Dab2-dependent LDLR endocytosis. We used siRNA to Dab2 and AP2 to block both the Dab2 and ARH-AP2 routes for LDLR endocytosis and assayed rescue by wild-type and mutant Dab2 (Figure 3A). These experiments were done in HeLa cells stably expressing an HA-tagged mini-LDLR (Li *et al*., 2001; Maurer and Cooper, 2006). Anti-HA antibodies were added to the cells at 37°C and uptake was allowed for 2 min. As expected, depletion of Dab2 and AP2 inhibited LDLR endocytosis, which was rescued by wild-type T7-p96 but not by T7-p67 (Figure 3, B and C). T7-Dab2-DPF* only weakly rescued endocytosis, suggesting that the Dab2-FCHO2 interaction is needed when AP2 levels are low (Figure 3A).

We also tested whether the interaction of Dab2 with FCHO2 is required when AP2 is present. We depleted cells of Dab2 and ARH to inactivate both the Dab2 and ARH-AP2 pathways, leaving AP2 at normal level (Figure 3, D and E; Keyel *et al*., 2006; Maurer and Cooper, 2006). Under these conditions, T7-p96 rescued LDLR endocytosis, but T7-p67 did not, as expected (Maurer and Cooper, 2006). With AP2 present, T7-Dab2-DPF* also rescued LDLR endocytosis (Figure 3, D and E). This indicates that AP2 is able to compensate for loss of the interaction between Dab2 and FCHO2. Taken together, these results suggest that the Dab2-FCHO2 interaction is not required for LDLR clustering in CCPs but is required for endocytosis of Dab2-specific cargo when AP2 is absent.

FCHO2 depletion affects the organization of CCP components and inhibits CME

As an alternative approach to understanding the role of FCHO2 in endocytosis, we depleted FCHO2 from HeLa cells using FCHO2 siRNA. Although we were unable to detect endogenous FCHO2

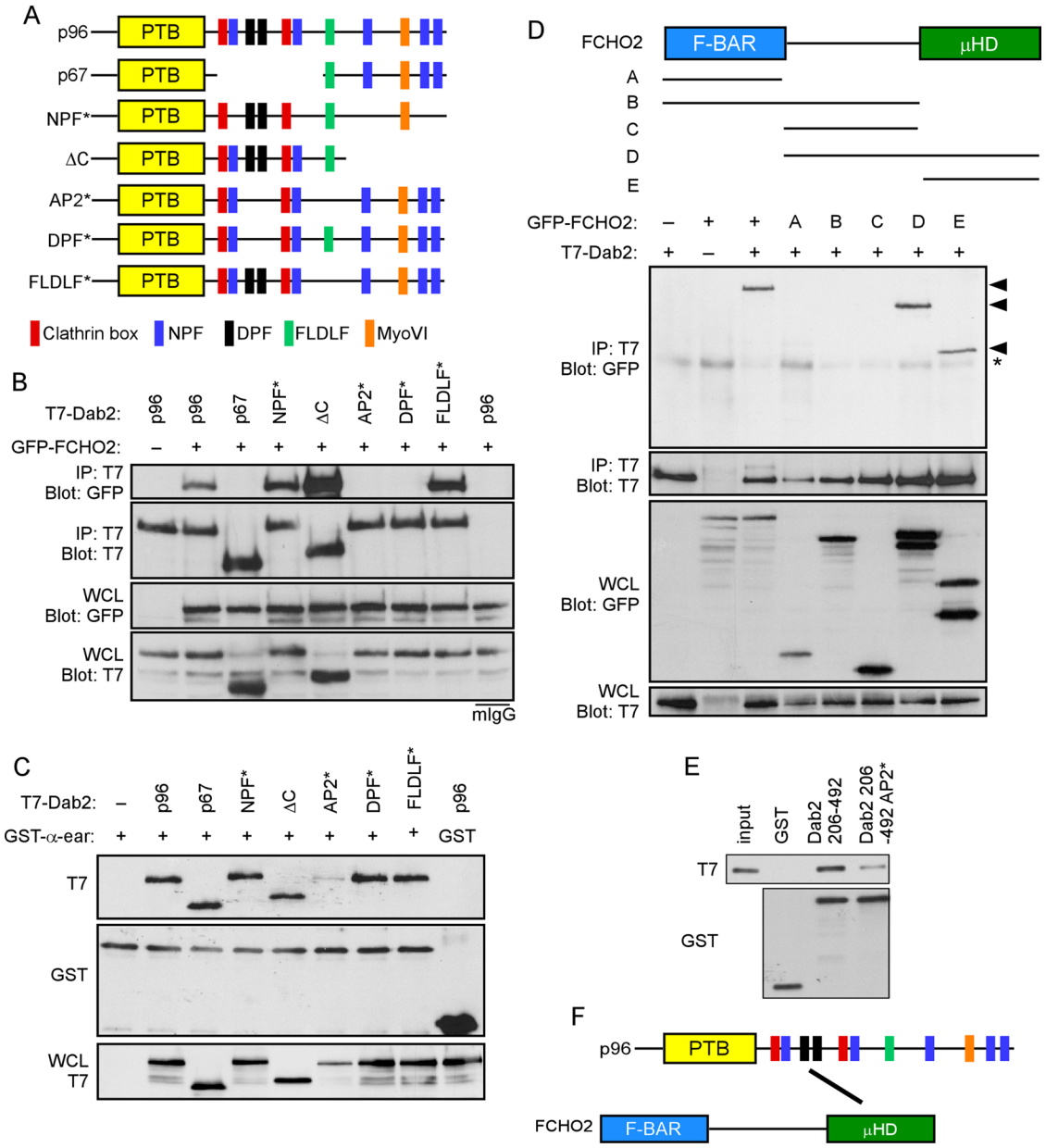

FIGURE 2: The Dab2 DPF motifs interact with the FCHO2 μHD. (A) Schematic of Dab2 structure and mutants. p96: full-length; p67: splice form lacking amino acids 229–447; NPF*: all five NPFs changed to NPV; ΔC: truncation after amino acid 576; AP2*: two DPFs changed to DAF and FLDLF changed to ALALF; DPF*: two DPFs changed to DAF; FLDLF*: FLDLF changed to ALALF. (B) Coimmunoprecipitation of GFP-FCHO2 with T7-tagged forms of Dab2. HeLa cells were transiently transfected with full-length GFP-FCHO2 and T7-tagged Dab2. Cells were lysed 48 h after transfection and immunoprecipitated with antibody to T7. (C) Binding of Dab2 mutants to AP2-α-ear. Cells were transiently transfected with T7-tagged Dab2 and lysed. Lysates were then mixed with purified, glutathione Sepharose–bound GST-AP2-α-ear. (D) Top, schematic of FCHO2 structure. FCHO2 contains an N-terminal F-BAR domain (residues 1–280), a central area (residues 281–520), and a C-terminal μHD (residues 521–810). FCHO2 constructs and amino acids as follows: A, amino acids 1–280; B, amino acids 1–520; C, amino acids 281–520; D, amino acids 281–810; and E, amino acids 521–810. Bottom, coimmunoprecipitation of GFP-FCHO2 forms with T7-Dab2. HeLa cells were transiently transfected with GFP-FCHO2 and full-length T7-p96. Cells were lysed 48 h after transfection and immunoprecipitated with antibody to T7. Arrowheads indicate GFP-tagged FCHO2 forms that coimmunoprecipitated with T7-Dab2. *, nonspecific band. (E) Binding of purified Dab2 and FCHO2 μHD. Purified, bacterially grown T7-FCHO2 μHD-His was mixed with purified, glutathione Sepharose–bound GST-Dab2 (residues 206–492). (F) The Dab2 DPF motifs (black) interact directly with the FCHO2 μHD.

protein using available antibodies, reverse transcriptase PCR (RT-PCR) showed that FCHO2 mRNA levels were considerably reduced upon siRNA treatment (Figure 4A). FCHO2 siRNA also inhibited expression of transfected GFP-FCHO2 (Figure 4A). FCHO2 siRNA induced a striking change in the number and size of CCSs, particularly on the adherent surface of the cell. There was a noticeable increase in the size of large structures that contained Dab2, AP2, and clathrin light chain-GFP (LCa-GFP; Figure 4B). These

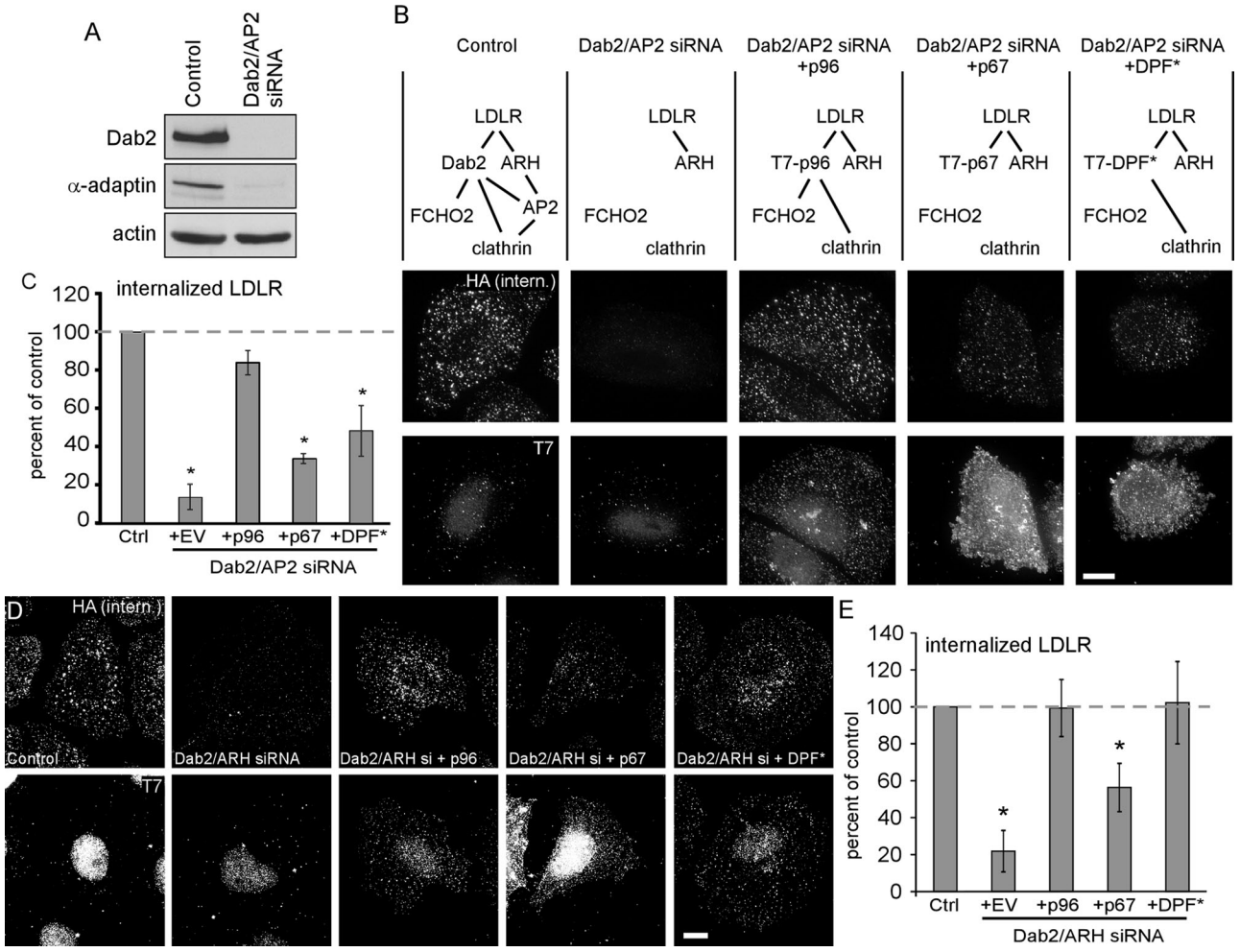

FIGURE 3: Disruption of the Dab2-FCHO2 interaction inhibits Dab2-dependent LDLR endocytosis when AP2 is depleted. (A) Dab2 and AP2 are efficiently depleted from HeLa-mini-LDLR cells with siRNA. Cells were transfected with siRNA to Dab2 and AP2 μ2 on days 1 and 3 and lysed for Western blotting on day 5. (B) Dab2-DPF* does not function for LDLR endocytosis in cells with low AP2 levels. HeLa-mini-LDLR cells were transfected with siRNA to Dab2 and AP2 or buffer control. The cells were then transfected with DNA encoding T7-tagged Dab2 p96 or p67 or DPF-mutant p96 (DPF*). Antibody to HA-mini-LDLR was added for 2 min at 37°C to measure receptor uptake. Fixed and permeabilized cells were stained with anti-T7 and appropriate secondary antibodies for anti-T7 (bottom row) and internalized anti-HA (top row). Only cells that were transfected with T7-Dab2 contain specific T7 staining; nuclear staining is background. Images are Z-stack projections. Scale bar: 10 μm. (C) Means and SEs of fluorescence intensity of at least five cells from three separate experiments are shown. *, $p < 0.05$ by Student's *t* test compared with control cells. Dashed line indicates control level; EV: empty vector. (D) Dab2-DPF* functions normally for LDLR endocytosis in cells with normal AP2. HeLa-mini-LDLR cells were transfected with siRNA to Dab2 and ARH or buffer control. The cells were then transfected with DNA encoding T7-tagged Dab2 p96 or p67 or DPF-mutant p96 (DPF*). Antibody to HA-mini-LDLR was added for 2 min at 37°C to measure receptor uptake. Fixed and permeabilized cells were stained with anti-T7 and appropriate secondary antibodies for anti-T7 (bottom row) and internalized anti-HA (top row). Images are Z-stack projections. Scale bar: 10 μm. (E) Means and SEs of fluorescence intensity of at least five cells from three separate experiments are shown. *, $p < 0.05$ by Student's *t* test compared with control cells. Dashed line indicates control level; EV: empty vector.

structures appeared similar to previously described large, flat clathrin arrays, called "clathrin plaques," found on the adherent surface of many cell types (Heuser, 1980; Maupin and Pollard, 1983; den Otter and Briels, 2011). Clathrin plaques are endocytically active (Saffarian *et al.*, 2009; Taylor *et al.*, 2011), although the mechanism is not thoroughly understood (Traub, 2011).

We quantified the numbers and sizes of Dab2-positive CCSs, defining plaques as structures with a diameter greater than 220 nm and pits as structures smaller than 220 nm (Anderson *et al.*, 1976; Traub, 2011). Depleting cells of FCHO2 reduced the number of pits and plaques by one-third but significantly increased plaque size (Table 1). Although the increase in median plaque size was modest, the distribution of plaque size showed a dramatic increase in the number of plaques greater than 300 μm^2 (Figure 4C). Similar results were obtained using AP2 as a marker for CCSs (unpublished data). This suggests that FCHO2 is important for the structural organization of CCS components.

To determine whether FCHO2 depletion affected endocytosis of Dab2 cargo, we measured uptake of HA-mini-LDLR. Control and FCHO2- or CHC-depleted cells were incubated at 37°C for 2 min with HA antibody. Depletion of FCHO2 and CHC inhibited LDLR internalization by 50 and 75%, respectively (Figure 4D). The

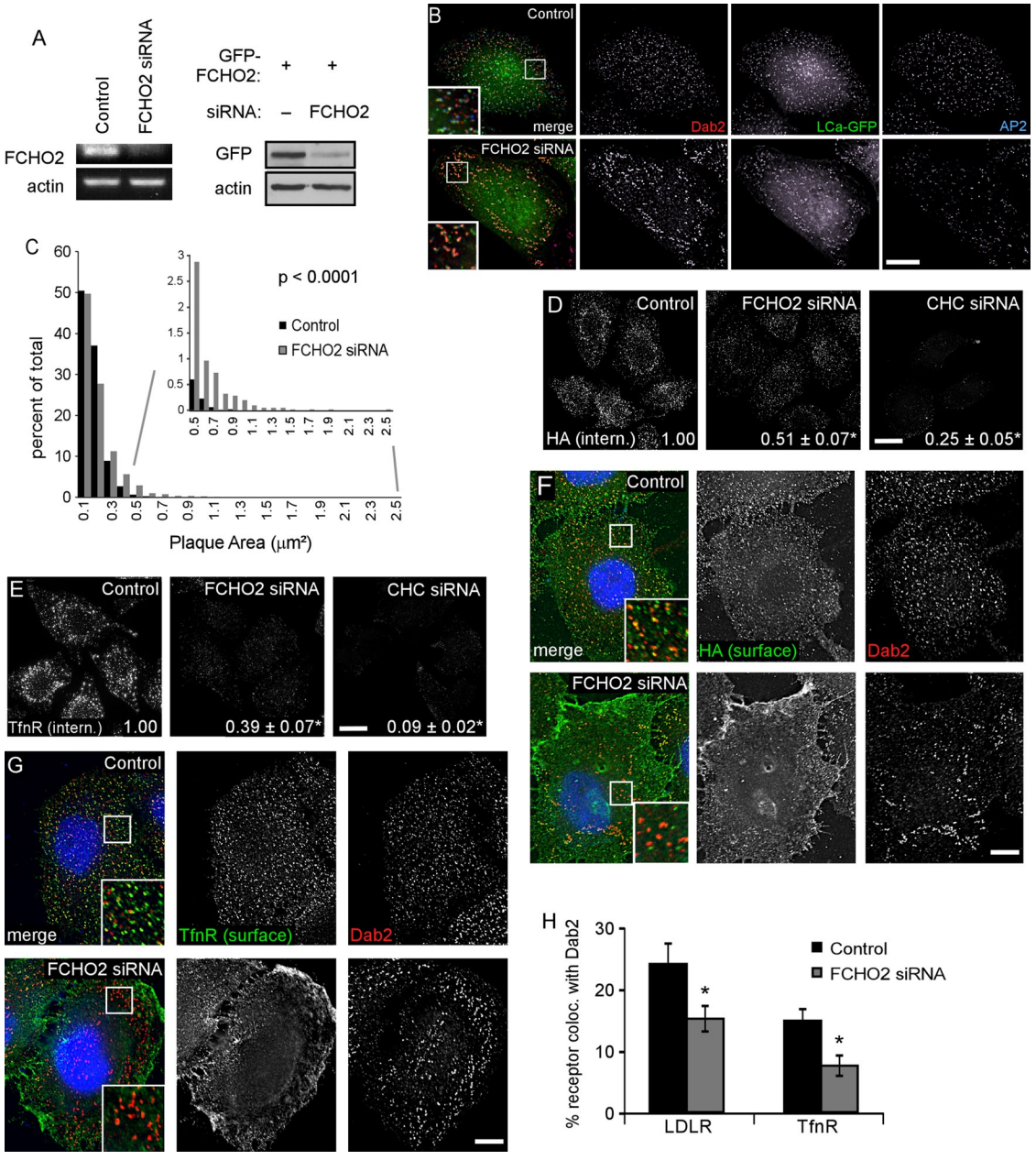

FIGURE 4: FCHO2 depletion affects the organization of CCP components and inhibits CME. (A) FCHO2 siRNA efficiently depletes FCHO2 from HeLa cells. Left, HeLa-mini-LDLR cells were transiently transfected with siRNA on days 1 and 3 and analyzed for mRNA levels by RT-PCR on day 5. Right, FCHO2 siRNA depletes GFP-FCHO2 from HeLa cells. Cells were transfected with FCHO2 siRNA on day 1, GFP-FCHO2 DNA on day 2, and FCHO2 siRNA again on day 3, and were lysed for Western blot on day 4. (B) Depletion of FCHO2 by siRNA induces large structures in HeLa cells. HeLa cells transiently transfected with FCHO2 siRNA and LCa-GFP were permeabilized and stained with antibodies to Dab2 and AP2. The bottom surface of the cell is shown. Scale bar: 10 μm. (C) Distribution of plaque size in FCHO2-depleted cells shows an increase in the occurrence of large structures on their adherent surfaces compared with control cells. The size of Dab2-positive structures with diameters larger than 220 nm was measured using ImageJ. The data shown is from a representative experiment. p value was calculated using the Mann-Whitney U test. (D and E) Depletion of FCHO2 by siRNA inhibits HA-mini-LDLR (D) and TfnR (E) endocytosis. Cells were given antibody against HA or TfnR and allowed to internalize for 2 min at 37°C. Values are mean fluorescence intensity ± SE of three experiments. Images are Z-stack projections. Scale bars: 20 μm. *, $p < 0.05$ by Student's *t* test compared with control. (F and G) Surface HA-mini-LDLR (F) and TfnR (G) fail to cluster into CCSs in FCHO2-depleted cells. Nonpermeabilized cells were stained with antibody to the extracellular domain of receptors, permeabilized, and stained with antibody to Dab2. Images are of the adherent surface of cells; blue is DAPI staining. Scale bars: 10 μm. (H) Colocalization of LDLR and TfnR with Dab2 at steady state. Using ImageJ, the percent area of surface receptor that colocalized with Dab2 was measured and mean and SEs were plotted. *, $p < 0.05$ by Student's *t* test.

	Median pit size (μm^2, n = 6)	Median plaque size (μm^2, n = 6)	CCSs per cell (n = 5)	CCPs per cell (n = 5)	Plaques per cell (n = 5)
Control	0.0247 ± 0.0003	0.112 ± 0.019	484 ± 101	159 ± 40	326 ± 34
FCHO2 siRNA	0.0227 ± 0.0020	0.133 ± 0.024	327 ± 48	107 ± 30	220 ± 23
p value	0.18	0.035	0.036	0.014	0.054

Dab2-positive structures were measured and quantified using ImageJ. Pits were defined as structures with diameters less than 220 nm and plaques as structures with diameters larger than 220 nm. Shown is mean ± SE from five fields from at least n experiments. p values were calculated using Student's *t* test.

TABLE 1: FCHO2 depletion decreases the number of CCSs and increases the size of clathrin plaques.

total amount of receptor was not changed by FCHO2 depletion (Figure S4). This indicates that FCHO2 is needed for efficient internalization of LDLR, a Dab2 cargo.

To determine whether FCHO2 is also required for Dab2-independent cargo, we measured internalization of TfnR. Depletion of FCHO2 and CHC inhibited TfnR internalization by 60 and 90%, respectively (Figure 4E; Uezu *et al.*, 2011). Although only a small amount of FCHO1 RNA was detected by RT-PCR (34 cycles against 24 cycles for FCHO2), it was possible that residual internalization of TfnR or LDLR involved FCHO1 (Figure S5A). However, cells depleted of FCHO1 and 2 still contained enlarged plaques, and depletion of FCHO1 and 2 did not additionally inhibit internalization of TfnR or LDLR compared to FCHO2 depletion alone. (Figure S5, B–D). Taken together, these data suggest that FCHO2 is involved in the internalization of cargo by Dab2 and other adaptor proteins.

One reason for decreased endocytosis may be reduced receptor clustering in clathrin structures. Indeed, staining of cell surfaces revealed that LDLR and TfnR were increased on the surface of FCHO2-depleted cells, and both receptors were more diffuse and not clustered in pits or plaques (Figure 4, F and G). There were significant decreases in the percentage of surface receptors that colocalized with Dab2 in CCSs when FCHO2 was depleted (Figure 4H). Taken together, these data suggest that FCHO2 plays an important, though not essential, role in CME and may be involved both in organizing CCSs and recruiting receptors to them.

Endocytic activity of enlarged CCSs

Clathrin plaques are reportedly active in endocytosis, either by budding off normal-sized CCVs or by bulk internalization of the entire plaque at once, utilizing the same protein components as canonical CCPs (Perrais and Merrifield, 2005; Saffarian *et al.*, 2009; Taylor *et al.*, 2011; Traub, 2011). Since FCHO2 depletion increased the size of clathrin structures and prevented receptor entry into them, we suspected this correlated with a defect in the early, receptor-recruitment steps of endocytosis. However, we wondered whether FCHO2-deficient plaques could internalize. It is well established that cargo recruitment continues at 4°C, even though budding is inhibited (Willingham *et al.*, 1981; Goldenthal *et al.*, 1984). Therefore we reasoned that incubation at 4°C might provide time for cargo recruitment to FCHO2-deficient CCSs, allowing us to measure internalization after warming to 37°C. Indeed, preincubation at 4°C for 1 h allowed surface LDLR to move from its diffuse localization at 37°C (Figure 4F) and become more concentrated in CCPs and plaques (Figure 5A). This movement was apparent in both control and FCHO2-depleted cells (Figures 4H and 5E). Preincubation at 4°C therefore allows LDLR to accumulate in enlarged clathrin structures in FCHO2-depleted cells and suggests a defect in receptor trapping by enlarged plaques.

We then warmed 4°C preincubated cells to 37°C and measured endocytosis. Under these conditions, depletion of FCHO2 or of both FCHO2 and FCHO1 did not significantly inhibit LDLR internalization (Figures 5B and S6A). Previous results indicated that LDLR endocytosis after 4°C preincubation occurs via either the Dab2 or ARH-AP2 pathway (Maurer and Cooper, 2006). Accordingly, endocytosis of preclustered receptors from enlarged plaques of FCHO2-deficient cells was not greatly affected by depleting AP2 or Dab2 (Figure S7). Therefore LDLR endocytosis occurs efficiently in FCHO2-depleted cells via the AP2 or Dab2 pathways, provided that LDLRs are given time to accumulate in CCSs before internalization is measured.

If FCHO2-deficient plaques are in fact internalizing LDLR, then the quantity of LDLR located in plaques should decrease after warming to 37°C. Cells were incubated with antibody against HA-mini-LDLR at 4°C for 1 h and then either fixed or warmed for 2 min at 37°C. Surface LDLR was visualized using immunofluorescence. Control cells that had been warmed for 2 min had a 24% decrease in LDLR intensity in CCSs on the adherent surface compared with cells that had not been warmed (Figure 5F). FCHO2-depleted cells had a 29% decrease in LDLR intensity in CCSs, including the large plaques, after warming. This decrease in intensity suggests that the receptor clustered into clathrin plaques during the 4°C incubation was, in fact, internalized during the 37°C incubation. Indeed, endocytic vesicles containing LDLR colocalized with large clathrin plaques of FCHO2-depleted cells (Figure 5F, blue channel). These results indicate that the large CCSs in FCHO2 are endocytically active.

Surprisingly, different results were obtained with the TfnR. Preincubation at 4°C did not increase the colocalization of TfnR with Dab2-positive CCSs (Figure 5, C and E), and there was still a significant 50% decrease in the amount of TfnR internalized under these conditions (Figure 5D). Again, we found no change in the amount of TfnR internalized with additional depletion of FCHO1 compared with FCHO2 siRNA alone (Figure S6B). This suggests that FCHO-deficient clathrin structures have a defect in clustering and internalizing TfnRs. Taken together, these data indicate that the plaque-like structures formed under conditions of depleted FCHO2 are able to internalize, but some receptors are recruited inefficiently.

DISCUSSION

We identified the F-BAR protein FCHO2 as a binding partner for the endocytic adaptor Dab2 and found that the Dab2 DPF motifs directly interact with the FCHO2 μHD. LDLR endocytosis is known to occur by parallel pathways, one of which is Dab2-dependent and one of which is dependent upon ARH-AP2 but not Dab2. Disruption of the Dab2-FCHO2 interaction decreased the uptake of LDLR in AP2-deficient cells, but not ARH-deficient cells, suggesting that Dab2 needs to bind to FCHO2 when AP2 levels are low. Dab2 may provide an alternative to AP2 for recruiting or stabilizing FCHO2 in CCSs. We also found that FCHO2 regulates the size and number of CCSs. Depletion of FCHO2 decreased the number of pits but

increased the size of larger CCSs, which are probably clathrin plaques. These larger plaques contained less of the Dab2 cargo LDLR and of the Dab2-independent cargo TfnR under physiological conditions, and endocytosis of both cargoes was inhibited. However, LDLR endocytosis was restored when FCHO2-deficient cells were preincubated at 4°C to accumulate receptor into plaques, suggesting that enlarged, FCHO2-deficient plaques can internalize.

FCHO2 is a CCS-organizing protein

Our results suggest that FCHO2 stimulates the formation of clathrin structures and limits the growth of plaques: when FCHO2 was absent, the number of clathrin structures was reduced by approximately one-third and the size of the larger plaques increased dramatically. Clathrin-dependent endocytosis of LDLR was also inhibited, but was rescued by simply preincubating the FCHO2-deficient cells in the cold before assay, suggesting that FCHO2 is not needed for internalization per se. Our HeLa cells contained very little FCHO1 RNA, and results obtained with cells depleted of both FCHO1 and FCHO2 were very similar to those obtained when FCHO2 alone was depleted. Overall, our results suggest that FCHO1/2 limit the size of plaques and/or enforce the curvature of clathrin lattices. It is perhaps not surprising that proteins that bind curved membranes, like FCHO1/2, would regulate lattice curvature. However, our conclusions contrast with a recent study reporting that depletion of FCHO1/2 completely inhibited the initiation of all clathrin structures (Henne *et al.*, 2010). The reason for the different results is not clear. Most experiments in the previous report used BSC1 cells, which are unusual in that they lack clathrin plaques. Our HeLa cells, like many other cell types, have plaques on their ventral, adherent surface (Heuser, 1980; Ehrlich *et al.*, 2004; Saffarian *et al.*, 2009). Also, HeLa cells express Dab2, while BSC1 cells only have very low levels of the protein (Maurer and Cooper, 2006; Mettlen *et al.*, 2010). The differences may also be technical. Our inability to detect either endogenous FCHO1 or FCHO2 with available antibodies means that small amounts of FCHO1/2 may have remained. Thus it is possible that low levels of FCHO1/2 reduce the number of pits and plaques and cause larger plaques, while complete absence of FCHO1/2 may completely inhibit clathrin assembly, as reported (Henne *et al.*, 2010). Alternatively, another protein that functionally overlaps with FCHO1/2 may be present in our HeLa cells.

In our hands, the absence of FCHO2 also inhibited the recruitment of receptors into clathrin structures. This inhibition could be a relatively trivial consequence of the altered number and size of plaques. When there are fewer, larger structures, there is more distance between them, so receptors freely diffusing on the membrane have a longer random walk before being trapped. The ability of FCHO-deficient plaques to accumulate LDLR after preincubation in the cold is consistent with this physical explanation. However, a purely physical explanation may not explain why FCHO2-deficient enlarged structures were unable to accumulate TfnR, even after preincubation at 4°C (Figure 5). FCHO2-depleted cells showed a lower ratio of AP2 to Dab2 in enlarged structures than in control CCSs (Figure 4B). This could affect recruitment of TfnR, an AP2 cargo. It also suggests that the plaques that grow when FCHO2 is absent somehow incorporate more Dab2 than AP2. A defect in receptor recruitment may explain the absence of all clathrin structures in the experiments of Henne *et al.* (2010). Empty CCPs are thought to abort prematurely (Loerke *et al.*, 2009). If CCPs in FCHO1/2 cells are unable to recruit cargo, they may abort prematurely.

We found that FCHO2-depleted cells internalized LDLR provided they were preincubated in the cold before warming and measuring internalization. This suggests that the enlarged FCHO2-deficient plaques are endocytically active, although we cannot exclude unanticipated effects of the preincubation. Temperature shifts were recently reported to induce artifactual membrane scission (Romer *et al.*, 2010), although this was clathrin independent and LDLR endocytosis in FCHO2-depleted cells was clathrin dependent (Figure 5). Therefore, although we cannot exclude experimental artifacts, we favor the interpretation that FCHO2-deficient plaques can internalize.

Requirement for the Dab2-FCHO2 complex

Mutation of the DPF motifs of Dab2 inhibited LDLR endocytosis when AP2, but not ARH, was depleted from cells (Figure 3). This indicates that the interaction between Dab2 and a DPF-interacting protein is essential for Dab2 function when AP2 levels are low. This DPF-interacting protein is likely FCHO2. While this requirement is only revealed under artificial conditions, its discovery adds to the understanding of the complex interactions occurring within a CCP.

Our finding that full-length, wild-type Dab2 was able to rescue LDLR endocytosis at physiological conditions in cells depleted of AP2 and Dab2 (Figure 3, A and B) was surprising, as there have been reports that AP2 is required for CCP formation (Boucrot *et al.*, 2010). AP2 may not be completely absent from our cells, just reduced low enough to inhibit the alternate ARH-AP2 route for LDLR endocytosis. We think it likely that modest overexpression of Dab2 is able to compensate for low levels of AP2 and permit receptor accumulation and endocytosis. Under these conditions, the FCHO2-interacting DPF motifs are needed, suggesting that Dab2 can substitute for AP2 and recruit or stabilize FCHO2 in clathrin structures.

Since preincubation in the cold rescued LDLR endocytosis in FCHO2-depleted cells (Figure 5), we wondered whether preincubation might rescue LDLR endocytosis by DPF*-mutant Dab2 in AP2-deficient cells. Surprisingly, it did not (Figure S8). How can these results be reconciled? The FCHO2-depleted cells have enlarged plaques, whereas Dab2-DPF* was assayed in cells with normal pits and plaques. Perhaps canonical pits and plaques require a Dab2-FCHO2 complex when AP2 levels are low, but enlarged plaques do not. This could suggest a fundamental difference between normal endocytic structures and those created upon FCHO2 depletion. Enlarged plaques may be a compensation mechanism upon loss of membrane-bending proteins to prevent a block of CME.

The DPF as a μHD-interacting motif

DPF motifs have been shown to bind AP2, but we show here that the DPF motifs of Dab2 also interact with the μHD of FCHO2 (Figure 2). DPF motifs exist in many proteins, including Eps15, auxilin, amphiphysin, AP180, synaptojanin, and HIP1 (Brett *et al.*, 2002). This raises the possibility that FCHO2 also binds to these other proteins through DPF sequences. In fact, Eps15, which binds to the FCHO2 μHD (Henne *et al.*, 2007), contains the sequence DPFKDDPF, which is highly similar to the DPFRDDPF sequence of Dab2. The abundance of proteins containing DPF motifs raises the possibility that many additional proteins may also interact with FCHO2 through their DPF motifs. The μHD of FCHO2 is a novel binding domain for DPF motifs, and this presents the possibility of competitive binding of DPF proteins by FCHO2 and AP2, thereby regulating interactions within a coated pit. Additionally, sequential binding of FCHO2 and AP2 to DPF sequences could play a role in the advancement of a CCP from one stage to another, for example from pit initiation to cargo recruitment.

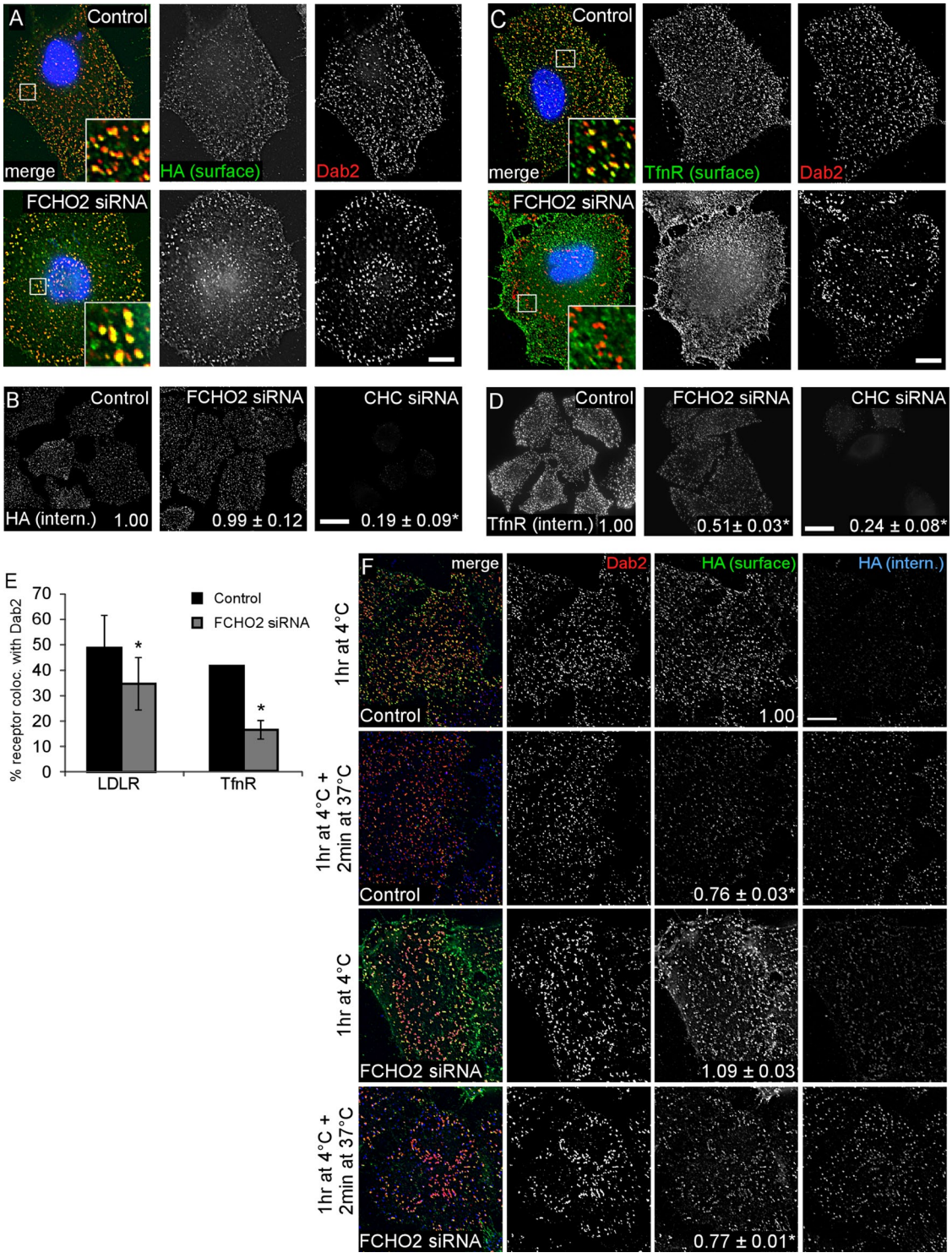

FIGURE 5: Endocytic activity of enlarged CCSs. (A) Incubation at 4°C allows HA-mini-LDLR to cluster into enlarged plaques. Control or FCHO2 siRNA-treated HeLa-mini-LDLR cells were fixed, stained with antibody to HA, permeabilized, and then stained with antibody to Dab2. Images are adherent surface of cells. Scale bar: 10 μm. (aCHO2 is dispensable for LDLR endocytosis when cells are preincubated at 4°C for 1 h. HeLa mini-LDLR cells were incubated with antibody to HA for 1 h at 4°C, washed, warmed to 37°C for 2 min, then cooled, acid-stripped, and permeabilized, and HA-LDLR uptake was visualized using immunofluorescence. Values are mean fluorescence intensity ± SE of three experiments. Images are Z-stack projections. Scale bar: 20 μm. *, $p < 0.05$ by Student's *t* test. (C) TfnR fails to localize to enlarged CCSs with a 4°C incubation. Control or FCHO2 siRNA-treated HeLa-mini-LDLR cells were fixed, stained with antibody to TfnR, permeabilized, and then stained with antibody to Dab2. Images are adherent surface of cells. Scale bar: 10 μm. (D) Depletion of FCHO2 inhibits TfnR endocytosis even with a 4°C preincubation. HeLa-mini-LDLR cells were incubated with antibody to TfnR for 1 h at 4°C, washed, and moved to 37°C for 2 min to measure TfnR uptake. Values are mean fluorescence intensity ± SE of three experiments. Images are Z-stack projections. Scale bar: 20 μm. *, $p < 0.05$ by Student's *t* test. (E) Colocalization of LDLR and TfnR with Dab2 after 1 h at 4°C incubation. Using ImageJ, the percent

MATERIALS AND METHODS

Cells

HeLa and BSC1 cells were cultured in DMEM, 10% fetal bovine serum, 1% penicillin–streptomycin in 37°C at 5% CO_2. HeLa cells stably expressing Dab2 shRNA have been previously described (Teckchandani *et al.*, 2009) and were maintained with the addition of 400 μg/ml hygromycin B. HeLa cells expressing HA-tagged mini-LDLR have also been described (Maurer and Cooper, 2006) and were cultured with 2 μg/ml puromycin.

Plasmids and transfection

T7-p96 and T7-p67 have been described (Maurer and Cooper, 2006), as has the C-terminal truncation mutant (Morris and Cooper, 2001). Point mutations in the NPF, DPF, and FLDLF motifs were created using site-directed mutagenesis. NPF was mutated to NPV (Doria *et al.*, 1999), DPF to DAF, and FLDLF to ALALF. FCHO1 (accession #BC028021) and FCHO2 (accession #BC137070) cDNAs were obtained from Open Biosystems (Rockford, IL) and cloned into the EcoRI sites of the pGL1-superC vector, creating an N-terminal GFP fusion product. GFP-FCHO2 constructs of amino acids 1–280, 281–520, 521–810, 1–520, and 281–810 were created by PCR and also cloned into pGL1-superC. GST-Dab2-206-492 has been described, and mutations in the AP2-binding sites were created in the same manner as for T7-p96-AP2*. For bacterial expression, FCHO2 cDNA was cloned into pET21a(+) (EMD Biosciences, Darmstadt, Germany). GST-AP2 α-ear was a gift from Harvey McMahon (MRC Laboratory of Molecular Biology, Cambridge, UK; Owen *et al.*, 1999). pQCXIP-HBT was from Peter Kaiser (University of California, Irvine, CA; Tagwerker *et al.*, 2006). LCa-GFP was a gift from Mark Von Zastrow (University of California, San Francisco, CA; Puthenveedu and von Zastrow, 2006). shRNA-resistant p96 was created using site-directed mutagenesis and the following primers: 1) CAGGGACAACACAAGCAGAGAATATGGGTCAACATTTCCTTGTCTGGCATAand2)CAACACAAGCAGAGAATATGGGTTAATATATCCTTGTCTGGCATAAAAATCATT, and reverse complements and inserted C-terminal to the HBT of pQCXIP-HBT. All DNA transfections were performed with Lipofectamine 2000 (Invitrogen, Carlsbad, CA) or GeneIn (GlobalStem, Rockville, MD), according to the manufacturers' protocols.

Antibodies

The following primary antibodies were used: mouse anti-HA.11 (Covance, Princeton, NJ), rabbit anti-GFP (Invitrogen), mouse anti-TfnR (Abcam, Cambridge, MA), rabbit anti-Dab2 (Santa Cruz Biotechnology, Santa Cruz, CA), mouse anti-p96 (BD Transduction Laboratories, East Rutherford, NJ), mouse anti-T7 (Novagen), mouse anti–α-adaptin AP6 (Calbiochem [San Diego, CA] and Abcam), mouse anti-ERK (BD Transduction Laboratories), goat anti-actin (Santa Cruz Biotechnology), goat anti-GST (GE Healthcare, Waukesha, WI), and rabbit anti-Eps15 (Santa Cruz Biotechnology). Appropriate Alexa Fluor–tagged secondary antibodies were used for immunofluorescence (Invitrogen) and HRP-tagged antibodies were used for Western blotting (GE Healthcare).

Mass spectrometry

Retroviral particles were produced by transfecting HEK293T cells with pQCXIP-HBT or pQCXIP-HBT-p96-resistant and an amphotropic packaging vector using calcium phosphate. Virus was harvested and used to infect HeLa cells stably expressing Dab2 shRNA. Cells were selected 48 h postinfection with 2 μg/ml puromycin and cloned. A clonal line that expressed p96 at high levels was isolated. Before being lysed for protein purification, cells were treated with 1 μM biotin in their cell culture media for 24 h to increase biotinylation levels.

Three 15-cm dishes of cells were lysed for protein purification in lysis buffer (50 mM Tris-HCl, pH 8.0, 100 mM NaF, 30 mM sodium pyrophosphate, 2 mM sodium molybdate, 1% NP-40, 2 mM sodium orthovanadate, and protease inhibitors [Roche]), sonicated, centrifuged 10 min at 14,000 × *g*, and rotated with nickel beads for 1.5 h at 4°C. Beads were then washed three times in lysis buffer and once in lysis buffer including 20 mM imidazole. Proteins were eluted in elution buffer (0.3 M NaCl, 0.5 M imidazole, 50 mM NaH_2PO_4, 10 mM EDTA, protease inhibitors, pH 7.9) by rotating beads for 10 min at room temperature in 500 μl elution buffer. The elution was repeated, and the eluates were combined. The eluate was then added to streptavidin beads washed in lysis buffer and rotated for 1.5 h at 4°C. Beads were washed five times in lysis buffer and resuspended in 50 μl Laemmli buffer. After SDS–PAGE on 4–12% gradient gels (Bio-Rad, Hercules, CA), entire gel lanes were excised.

Individual gel slices in 1.5 ml tubes (Eppendorf) were subjected to consecutive 15-min washes with: water, 50% acetonitrile, 100% acetonitrile, 100 mM ammonium bicarbonate, and 50% acetonitrile in 50 mM ammonium bicarbonate. After the final wash solution was removed, the gel slices were dried thoroughly by vacuum centrifugation. The gel slices were then cooled on ice, and an ice-cold solution of 12.5 ng/μl sequencing grade trypsin (Promega, Madison, WI) in 50 mM ammonium bicarbonate was added to the gel slices, which were then incubated on ice for 1 h. The trypsin solution was discarded and replaced with 50 mM ammonium bicarbonate and the gel slices were incubated overnight at 37°C. Following digestion, the supernatants were collected, and the gel slices were washed with 0.1% formic acid, which was followed by washing with 0.1% formic acid in 50% acetonitrile (30 min each wash). The original digestion supernatant and the washes for a single sample were combined into a single tube and dried by vacuum centrifugation. The digestion products were desalted using ZipTips (Millipore, Billerica, MA) per the manufacturer's instructions and dried by vacuum centrifugation.

Dried peptide mixtures were resuspended in 5 μl of 0.1% formic acid and analyzed by LC electrospray ionization MS/MS with a NanoLC-2D (Eksigent, Dublin, CA) coupled to LTQ-OrbiTrap mass spectrometer (ThermoElectron, Waltham, MA) using a "vented" instrument configuration, as previously described (Licklider *et al.*, 2002), and a solvent system consisting of 0.1% formic acid in water, and 0.1% formic in 100% acetonitrile. In-line desalting was accomplished using an IntegraFrit trap column (100 μm × 25 mm; New Objective,

of surface receptor area that colocalized with Dab2 area was measured, and mean and SEs were plotted. *, $p < 0.05$ by Student's *t* test. (F) Receptors are internalized from enlarged structures. HeLa-mini-LDLR cells were given antibody to HA-mini-LDLR for 1 h at 4°C and washed, and then were either fixed (1 h at 4°C) or warmed to 37°C for 2 min and fixed. Nonpermeabilized cells were stained with secondary antibody to surface HA-labeled receptor and then permeabilized and stained with anti-Dab2 and secondary antibodies for anti-Dab2 and internalized anti-HA–labeled receptor. Numbers on HA surface panels are mean fluorescence intensity ± SE of surface HA that colocalized with Dab2. Scale bar: 10 μm. *, $p < 0.05$ by Student's *t* test, compared with control after 1 h at 4°C.

Woburn, MA) packed with reverse-phase Magic C18AQ (5 μm 200 Å resin; Michrom Bioresources, Auburn, CA), followed by peptide separations on a PicoFrit column (75 μm × 200 mm; New Objective) packed with reverse phase Magic C18AQ (5-μm 100 Å resin; Michrom Bioresources) directly mounted on the electrospray ion source. A linear gradient was used starting at 2% B and proceeding to 40% B in 40 min. The acetonitrile percentage was increased to 90% B and held for 5 min, and then it was reduced to 2% B and held for 15 min. A flow rate of 400 nl/min was used for chromatographic separations, and the mass spectrometer capillary temperature was set to 200°C. A spray voltage of 2750 V was applied to the electrospray tip, and the LTQ-OrbiTrap instrument was operated in the data-dependent mode, switching automatically between MS survey scans in the OrbiTrap (AGC target value of 1,000,000; resolution of 60,000; ion time of 150 ms) with MS/MS spectra acquisition in the linear ion trap (AGC target value of 10,000; ion time of 100 ms). The five most intense ions from the Fourier-transform full scan were selected in the linear ion trap for fragmentation by collision-induced dissociation with normalized collision energy of 35%. Selected ions were dynamically excluded for 45 s.

The protein database search algorithm X!Tandem (Craig and Beavis, 2004) was used to identify peptides from the human (version 3.59) International Protein Index protein databases. Peptide false discovery rates were measured using Peptide Prophet (Keller *et al.*, 2002), and results were stored and analyzed in the Computational Proteomics Analysis System (Rauch *et al.*, 2006). Peptides were filtered with a minimum Peptide Prophet probability that produced a false discovery rate of ~5%, and the resulting peptides were grouped into proteins.

Immunoprecipitation

Cells were lysed in lysis buffer (150 mM NaCl, 10 mM HEPES, pH 7.4, 2 mM EDTA, 50 mM NaF, 1% Triton-X100, protease inhibitors), rotated at 4°C for 30 min, and centrifuged for 10 min at 14,000 × *g*. Protein concentrations were measured, and equal amounts of protein were used for immunoprecipitation. Lysate was rotated with primary antibody for 3 h at 4°C. Protein A+G beads (GE Healthcare) washed in lysis buffer were added to the lysate/antibody mixture and rotated for 1 h at 4°C. Beads were then washed in lysis buffer three times and resuspended in 5X Laemmli buffer before SDS–PAGE.

Protein purification and binding assays

GST-tagged proteins were induced in BL-21 with 0.1 mM isopropyl-β-D-thiogalactopyranoside for 3–4 h at 30°C with shaking. Cells were collected by centrifugation and resuspended in resuspension buffer (0.5% NP-40 and 1 mM dithiothreitol (DTT) in PBS with protease inhibitors). Lysozyme was added to a concentration of 0.5 mg/ml, and cells were lysed 15 min on ice. The lysates were then sonicated and centrifuged at 4000 × *g* for 20 min. Glutathione sepharose-4B beads (GE Healthcare) were washed twice in resuspension buffer and added to the lysates. After rotation at 4°C for 1.5 h, beads were washed twice in resuspension buffer with 350 mM NaCl and three times in resuspension buffer. Beads were aliquoted and snap frozen in resuspension buffer with the addition of 5% glycerol.

His-tagged FCHO2-μHD was purified similarly (Boettner *et al.*, 2009), with the following changes. Protein expression was induced at 22°C for 3 h, and the bacterial pellet was resuspended in resuspension buffer with the addition of 20 mM imidazole (pH 8.0). After incubation of the lysate with glutathione Sepharose beads, the beads were washed twice in resuspension buffer with 350 mM NaCl and 15 mM imidazole, and then washed three times in resuspension buffer with 15 mM imidazole. Beads were then loaded into an empty Bio-Rad poly-prep column and eluted with increasing concentrations of imidazole ranging from 50–200 mM. The majority of T7-FCHO2-μHD-His was eluted with 100 mM imidazole, and protein from this fraction was used for binding experiments.

For Dab2-FCHO2 binding experiments, 150 ng of T7-μHD-His was mixed with the same amount of glutathione Sepharose–bound GST-Dab2, and the volume was increased to 500 μl with Buffer A (50 mM Tris, pH 8.0, 150 mM NaCl, 1 mM EDTA, 0.5% Triton X-100, and protease inhibitors). After 1.5 h rotating at 4°C, beads were pelleted, washed twice in Buffer A with 500 mM NaCl, washed three times in Buffer A, and resuspended in 120 μl 5X Laemmli sample buffer. Two microliters of this volume were used for SDS–PAGE and Western blotting.

For GST-α-ear:Dab2 binding, T7-tagged Dab2 constructs were transiently transfected into HeLa cells, which were lysed in 150 mM NaCl, 20 mM HEPES (pH 7.2), 5 mM DTT, 0.1% Triton X-100, and protease inhibitors. Lysates were harvested, cleared by centrifugation, and incubated as above, with glutathione Sepharose-bound GST-α-ear. Beads were washed twice in Buffer A (50 mM Tris, pH 8.0, 150 mM NaCl, 1 mM EDTA, 0.5% Triton X-100, and protease inhibitors) with 500 mM total NaCl, three times in Buffer A, and resuspended as above.

siRNA

Pools of siRNA (siGENOME SMARTpool) against human AP2 μ2, Dab2, FCHO1, FCHO2, Eps15, Eps15R, ITSN1, and CHC were from Dharmacon, Lafayette, CO. ITSN2 siRNA was from Santa Cruz Biotechnology. For rescue experiments, a single Dab2 siRNA (Dharmacon) that targets human, but not mouse, Dab2 (AAAGGGTGAAGGCUGGUUCUU) was used so rescues could be performed using mouse Dab2 sequences. siRNA (50 pmol) was transfected into cells using Oligofectamine (Invitrogen) according to the manufacturer's protocol. Cells plated on 2 μg/ml collagen IV (Sigma-Aldrich, St. Louis, MO) were transfected with siRNA on day 1, transfected again on day 3, and assayed on day 5. For Dab2 rescue experiments and immunoprecipitation from cells treated with siRNA, DNA was transfected on day 4 using Lipofectamine 2000 (Invitrogen). For assaying siRNA depletion of GFP-tagged FCHO constructs, cells were transfected with siRNA pools on day 1, transfected with DNA on day 2 using GeneIn (GlobalStem), transfected again with siRNA on day 3, and harvested on day 4.

Endocytosis

Endocytosis assays were performed essentially as described (Maurer and Cooper, 2006), with some modifications. For assays at 37°C, cells were removed from the 37°C incubator and washed quickly with PBS, and antibody was added in 37°C assay media (DMEM/F12, 0.1% bovine serum albumin [BSA], 10 mM HEPES, pH 7.4). The cells were immediately placed into a 37°C water bath for 2 min. Cells were then moved directly to 4°C, washed with cold PBS, acid-stripped (0.5 M NaCl, 0.2 M acetic acid) for 10 min, and fixed in cold 4% paraformaldehyde for 20 min.

For assays including a 4°C preincubation, cells were removed from 37°C to 4°C, washed in cold PBS, incubated with primary antibody in assay media for 1 h, and washed again in cold PBS. Prewarmed assay media was then added, and the cells were moved to a 37°C water bath for 2 min. Cells were then moved back to 4°C and acid-stripped and fixed as above.

Immunofluorescence

Cells grown on collagen IV–coated glass coverslips were fixed in 4% paraformaldehyde for 20 min at room temperature and washed

three times in PBS. They were then permeabilized for 10 min in 0.1% Triton-X100 in PBS. Cells were washed in PBS and blocked for 1 h in 5% normal goat serum/2% BSA in PBS before primary antibody was added in blocking solution. After a 2 h incubation in primary antibody at room temperature, cells were washed, incubated for 1 h in Alexa Fluor–conjugated secondary antibody (Invitrogen) at room temperature and 4′,6-diamidino-2-phenylindole (DAPI) for 10 min. After several washes in PBS, coverslips were mounted on slides with ProLong Gold with antifade (Invitrogen).

Cells to be incubated at 4°C were removed from the tissue culture incubator to 4°C, washed in cold PBS, and incubated at 4°C for 1 h in endocytosis assay media. They were then washed in cold PBS and fixed for 20 min in cold 4% paraformaldehyde. For surface receptor staining, cells were blocked and incubated with appropriate primary and secondary antibodies for surface receptor before permeabilization. If necessary, remaining surface antibody was blocked with goat secondary antibody.

Microscopy and image quantification

Cells were imaged using an Olympus Deltavision IX70 deconvolution microscope or a Deltavision IX71 deconvolution microscope. All images were taken using a 60×, numerical aperture 1.42, oil objective with a Z-slice size of 0.2 µm. Images were acquired and deconvolved using SoftWorx (Applied Precision, Issaquah, WA), and all exposure times and image scaling were equal within an experiment. All quantification was done with ImageJ (National Institutes of Health, Bethesda, MD).

RT-PCR

RNA was harvested from cells using an RNeasy kit (Qiagen, Valencia, CA) according to the manufacturer's directions. cDNA was created using random primers (Invitrogen) and Superscript II reverse transcriptase (Invitrogen) according to the manufacturer's instructions. PCR was performed using the primers: 1) GAGCAGATCCCACCAAGTGT and 2) CAAGCTGTGCATTTGGAAGA for FCHO2, and 1) GCGAGAAGATGACCCAGATCATGTT and 2) GCTTCTCCTTAATGTCACGCACGAT for actin. Two sets of primers were used to detect FCHO1 cDNA: 1) AAGCCATGGAGGAGACACAC and TGACGTTCTCGATGTTCTGC and 2) ACCATGAAACGCCATTCTTC and TCTTGGACACCTGCTCCTCT.

ACKNOWLEDGMENTS

We thank Peter Kaiser, Valeri Vasioukhin, Wen-Hui Lien, Tomas Kirchhausen, Linton Traub, Mark Von Zastrow, Harvey McMahon, Anjali Teckchandani, other members of the Cooper laboratory, and the Fred Hutchinson Cancer Research Center Proteomics and Scientific Imaging resources for helpful discussions, reagents, and technical assistance. We also thank Anjali Teckchandani, Susan Parkhurst, Stephanie Busch, and Valeri Vasioukhin for critical reading of the manuscript. This work was supported by National Institute of Health grant R01-GM66257. E.E.M. was supported by the Viral Oncology Training Grant T32 CA009229.

REFERENCES

Anderson RG, Goldstein JL, Brown MS (1976). Localization of low density lipoprotein receptors on plasma membrane of normal human fibroblasts and their absence in cells from a familial hypercholesterolemia homozygote. Proc Natl Acad Sci USA 73, 2434–2438.

Benmerah A, Gagnon J, Begue B, Megarbane B, Dautry-Varsat A, Cerf-Bensussan N (1995). The tyrosine kinase substrate eps15 is constitutively associated with the plasma membrane adaptor AP-2. J Cell Biol 131, 1831–1838.

Boettner DR, D'Agostino JL, Torres OT, Daugherty-Clarke K, Uygur A, Reider A, Wendland B, Lemmon SK, Goode BL (2009). The F-BAR protein Syp1 negatively regulates WASp-Arp2/3 complex activity during endocytic patch formation. Curr Biol 19, 1979–1987.

Bonifacino JS, Traub LM (2003). Signals for sorting of transmembrane proteins to endosomes and lysosomes. Annu Rev Biochem 72, 395–447.

Boucrot E, Saffarian S, Zhang R, Kirchhausen T (2010). Roles of AP-2 in clathrin-mediated endocytosis. PLoS One 5, e10597.

Brett TJ, Traub LM, Fremont DH (2002). Accessory protein recruitment motifs in clathrin-mediated endocytosis. Structure 10, 797–809.

Calderwood DA, Fujioka Y, de Pereda JM, Garcia-Alvarez B, Nakamoto T, Margolis B, McGlade CJ, Liddington RC, Ginsberg MH (2003). Integrin β cytoplasmic domain interactions with phosphotyrosine-binding domains: a structural prototype for diversity in integrin signaling. Proc Natl Acad Sci USA 100, 2272–2277.

Conner SD, Schmid SL (2003). Regulated portals of entry into the cell. Nature 422, 37–44.

Craig R, Beavis RC (2004). TANDEM: matching proteins with tandem mass spectra. Bioinformatics 20, 1466–1467.

den Otter WK, Briels WJ (2011). The generation of curved clathrin coats from flat plaques. Traffic 12, 1407–1416.

Di Fiore PP, Pelicci PG, Sorkin A (1997). EH: a novel protein-protein interaction domain potentially involved in intracellular sorting. Trends Biochem Sci 22, 411–413.

Doria M, Salcini AE, Colombo E, Parslow TG, Pelicci PG, Di Fiore PP (1999). The eps15 homology (EH) domain-based interaction between eps15 and hrb connects the molecular machinery of endocytosis to that of nucleocytosolic transport. J Cell Biol 147, 1379–1384.

Ehrlich M, Boll W, Van Oijen A, Hariharan R, Chandran K, Nibert ML, Kirchhausen T (2004). Endocytosis by random initiation and stabilization of clathrin-coated pits. Cell 118, 591–605.

Goldenthal KL, Pastan I, Willingham MC (1984). Initial steps in receptor-mediated endocytosis. The influence of temperature on the shape and distribution of plasma membrane clathrin-coated pits in cultured mammalian cells. Exp Cell Res 152, 558–564.

He G, Gupta S, Yi M, Michaely P, Hobbs HH, Cohen JC (2002). ARH is a modular adaptor protein that interacts with the LDL receptor, clathrin, and AP-2. J Biol Chem 277, 44044–44049.

Henne WM, Boucrot E, Meinecke M, Evergren E, Vallis Y, Mittal R, McMahon HT (2010). FCHo proteins are nucleators of clathrin-mediated endocytosis. Science 328, 1281–1284.

Henne WM, Kent HM, Ford MG, Hegde BG, Daumke O, Butler PJ, Mittal R, Langen R, Evans PR, McMahon HT (2007). Structure and analysis of FCHo2 F-BAR domain: a dimerizing and membrane recruitment module that effects membrane curvature. Structure 15, 839–852.

Heuser J (1980). Three-dimensional visualization of coated vesicle formation in fibroblasts. J Cell Biol 84, 560–583.

Hussain NK, Yamabhai M, Ramjaun AR, Guy AM, Baranes D, O'Bryan JP, Der CJ, Kay BK, McPherson PS (1999). Splice variants of intersectin are components of the endocytic machinery in neurons and nonneuronal cells. J Biol Chem 274, 15671–15677.

Keller A, Nesvizhskii AI, Kolker E, Aebersold R (2002). Empirical statistical model to estimate the accuracy of peptide identifications made by MS/MS and database search. Anal Chem 74, 5383–5392.

Keyel PA, Mishra SK, Roth R, Heuser JE, Watkins SC, Traub LM (2006). A single common portal for clathrin-mediated endocytosis of distinct cargo governed by cargo-selective adaptors. Mol Biol Cell 17, 4300–4317.

Kowanetz K, Terzic J, Dikic I (2003). Dab2 links CIN85 with clathrin-mediated receptor internalization. FEBS Lett 554, 81–87.

Li Y, Lu W, Marzolo MP, Bu G (2001). Differential functions of members of the low density lipoprotein receptor family suggested by their distinct endocytosis rates. J Biol Chem 276, 18000–18006.

Licklider LJ, Thoreen CC, Peng J, Gygi SP (2002). Automation of nanoscale microcapillary liquid chromatography-tandem mass spectrometry with a vented column. Anal Chem 74, 3076–3083.

Loerke D, Mettlen M, Yarar D, Jaqaman K, Jaqaman H, Danuser G, Schmid SL (2009). Cargo and dynamin regulate clathrin-coated pit maturation. PLoS Biol 7, e57.

Maupin P, Pollard TD (1983). Improved preservation and staining of HeLa cell actin filaments, clathrin-coated membranes, and other cytoplasmic structures by tannic acid-glutaraldehyde-saponin fixation. J Cell Biol 96, 51–62.

Maurer ME, Cooper JA (2006). The adaptor protein Dab2 sorts LDL receptors into coated pits independently of AP-2 and ARH. J Cell Sci 119, 4235–4246.

McMahon HT, Boucrot E (2011). Molecular mechanism and physiological functions of clathrin-mediated endocytosis. Nat Rev Mol Cell Biol 12, 517–533.

Mettlen M, Loerke D, Yarar D, Danuser G, Schmid SL (2010). Cargo- and adaptor-specific mechanisms regulate clathrin-mediated endocytosis. J Cell Biol 188, 919–933.
Mishra SK, Keyel PA, Edeling MA, Dupin AL, Owen DJ, Traub LM (2005). Functional dissection of an AP-2 β2 appendage-binding sequence within the autosomal recessive hypercholesterolemia protein. J Biol Chem 280, 19270–19280.
Mishra SK, Keyel PA, Hawryluk MJ, Agostinelli NR, Watkins SC, Traub LM (2002a). Disabled-2 exhibits the properties of a cargo-selective endocytic clathrin adaptor. EMBO J 21, 4915–4926.
Mishra SK, Watkins SC, Traub LM (2002b). The autosomal recessive hypercholesterolemia (ARH) protein interfaces directly with the clathrin-coat machinery. Proc Natl Acad Sci USA 99, 16099–16104.
Morris SM, Arden SD, Roberts RC, Kendrick-Jones J, Cooper JA, Luzio JP, Buss F (2002). Myosin VI binds to and localises with Dab2, potentially linking receptor-mediated endocytosis and the actin cytoskeleton. Traffic 3, 331–341.
Morris SM, Cooper JA (2001). Disabled-2 colocalizes with the LDLR in clathrin-coated pits and interacts with AP-2. Traffic 2, 111–123.
Motley A, Bright NA, Seaman MN, Robinson MS (2003). Clathrin-mediated endocytosis in AP-2-depleted cells. J Cell Biol 162, 909–918.
Nishimura T, Kaibuchi K (2007). Numb controls integrin endocytosis for directional cell migration with aPKC and PAR-3. Dev Cell 13, 15–28.
Owen DJ, Vallis Y, Noble ME, Hunter JB, Dafforn TR, Evans PR, McMahon HT (1999). A structural explanation for the binding of multiple ligands by the α-adaptin appendage domain. Cell 97, 805–815.
Perrais D, Merrifield CJ (2005). Dynamics of endocytic vesicle creation. Dev Cell 9, 581–592.
Praefcke GJ, Ford MG, Schmid EM, Olesen LE, Gallop JL, Peak-Chew SY, Vallis Y, Babu MM, Mills IG, McMahon HT (2004). Evolving nature of the AP2 α-appendage hub during clathrin-coated vesicle endocytosis. EMBO J 23, 4371–4383.
Puthenveedu MA, von Zastrow M (2006). Cargo regulates clathrin-coated pit dynamics. Cell 127, 113–124.
Rauch A *et al*. (2006). Computational Proteomics Analysis System (CPAS): an extensible, open-source analytic system for evaluating and publishing proteomic data and high throughput biological experiments. J Proteome Res 5, 112–121.
Reider A, Barker SL, Mishra SK, Im YJ, Maldonado-Baez L, Hurley JH, Traub LM, Wendland B (2009). Syp1 is a conserved endocytic adaptor that contains domains involved in cargo selection and membrane tubulation. EMBO J 28, 3103–3116.
Romer W *et al*. (2010). Actin dynamics drive membrane reorganization and scission in clathrin-independent endocytosis. Cell 140, 540–553.
Saffarian S, Cocucci E, Kirchhausen T (2009). Distinct dynamics of endocytic clathrin-coated pits and coated plaques. PLoS Biol 7, e1000191.
Schmid EM, Ford MG, Burtey A, Praefcke GJ, Peak-Chew SY, Mills IG, Benmerah A, McMahon HT (2006). Role of the AP2 β-appendage hub in recruiting partners for clathrin-coated vesicle assembly. PLoS Biol 4, e262.
Tagwerker C, Flick K, Cui M, Guerrero C, Dou Y, Auer B, Baldi P, Huang L, Kaiser P (2006). A tandem affinity tag for two-step purification under fully denaturing conditions: application in ubiquitin profiling and protein complex identification combined with in vivo cross-linking. Mol Cell Proteomics 5, 737–748.
Taylor MJ, Perrais D, Merrifield CJ (2011). A high precision survey of the molecular dynamics of mammalian clathrin-mediated endocytosis. PLoS Biol 9, e1000604.
Teckchandani A, Toida N, Goodchild J, Henderson C, Watts J, Wollscheid B, Cooper JA (2009). Quantitative proteomics identifies a Dab2/integrin module regulating cell migration. J Cell Biol 186, 99–111.
Traub LM (2003). Sorting it out: AP-2 and alternate clathrin adaptors in endocytic cargo selection. J Cell Biol 163, 203–208.
Traub LM (2009). Tickets to ride: selecting cargo for clathrin-regulated internalization. Nat Rev Mol Cell Biol 10, 583–596.
Traub LM (2011). Regarding the amazing choreography of clathrin coats. PLoS Biol 9, e1001037.
Uezu A *et al*. (2007). SGIP1α is an endocytic protein that directly interacts with phospholipids and Eps15. J Biol Chem 282, 26481–26489.
Uezu A, Umeda K, Tsujita K, Suetsugu S, Takenawa T, Nakanishi H (2011). Characterization of the EFC/F-BAR domain protein, FCHO2. Genes Cells 16, 868–878.
Wang LH, Sudhof TC, Anderson RG (1995). The appendage domain of α-adaptin is a high affinity binding site for dynamin. J Biol Chem 270, 10079–10083.
Willingham MC, Rutherford AV, Gallo MG, Wehland J, Dickson RB, Schlegel R, Pastan IH (1981). Receptor-mediated endocytosis in cultured fibroblasts: cryptic coated pits and the formation of receptosomes. J Histochem Cytochem 29, 1003–1013.
Xu XX, Yang W, Jackowski S, Rock CO (1995). Cloning of a novel phosphoprotein regulated by colony-stimulating factor 1 shares a domain with the *Drosophila disabled* gene product. J Biol Chem 270, 14184–14191.
Xu XX, Yi T, Tang B, Lambeth JD (1998). Disabled-2 (Dab2) is an SH3 domain-binding partner of Grb2. Oncogene 16, 1561–1569.
Zhou J, Scholes J, Hsieh JT (2003). Characterization of a novel negative regulator (DOC-2/DAB2) of c-Src in normal prostatic epithelium and cancer. J Biol Chem 278, 6936–6941.